www.amlett.com, www.vbripress.com/aml, DOI: 10.5185/amlett.2015.5844 Published online by the VBRI Press in 2015

Synthesis and characterization of SnO_2 nanoparticles: Effect of hydrolysis rate on the optical properties

R. Bargougui[1*], K. Omri[2], A. Mhemdi[1], S. Ammar[1,3]

[1]*Faculty of Sciences of Gabes, Gabes University, Cite Erriadh 6072, Tunisia*
[2]*Laboratory of Physics of Materials and Nanomaterials Applied at Environment (LaPhyMNE), Gabes University, Faculty of Sciences in Gabes, Cite Erriadh 6072, Tunisia*
[3]*Faculty of Sciences of Bizerte, University Carthage, Jarzouna 7021, Tunisia*

[*]Corresponding author. Tel: (+21) 622934625; E-mail:bargougui_radhwane@yahoo.fr

Received: 10 February 2015, Revised: 15 May 2015 and Accepted: 17 May 2015

ABSTRACT

Nanocrystalline SnO_2 oxides particles have been successfully synthesized via polyol process using diethylene glycol (DEG) as a solvent, followed by powder thermal treatment. The general applicability of the process is shown and the advantages in terms of properties and processability are described. The powders thus prepared were investigated using X-ray diffractometry. (XRD), scanning electron microscopy (SEM), transmission electron microscopy (TEM), and photoluminescence spectra (PL). The X-ray diffraction patterns of the samples were indexed to the rutile phase for SnO_2.The TEM images show uniform isotropic morphologies with average sizes close to10 nm. This decrease in particle size is accompanied with a decrease in the band-gap value from 3.55 eV for SnO_2 down to 3.27 eV as shown by UV-visible spectra. It is demonstrated that the crystallite size less than 10 nm can be controlled by changing the quantity of added water (rate hydrolysis h=n H_2O/n Metal). Copyright © 2015 VBRI Press.

Keywords: SnO_2; nanoparticle; polyol method; optical materials; photoluminescence.

Introduction

In recent decades, the semiconductor nanocrystals are of significant interest and focus in the last decades with respect to their technological applications. The electrical, optical and magnetic properties of such particles are highly dependent on their particle size [**1, 2**]. A number of metal oxide nanostructures exhibiting attractive performances have been synthesized and reported recently [**3-6**].

Particularly, the tin dioxide (SnO_2) are wide band gap semi conducting materials used extensively as UV-absorbers, self-cleaning, gas sensors, and conductive inks [**7, 8**]. Such nanostructures are more attractive because their band gaps and thus electronic properties can be changed by chemical or structural modifications. Up to now, a variety of techniques have been developed to prepare nanoparticles, sol-gel method [**9, 10**], hydrothermal technique [**11**], chemical co-precipitation [**12**] and polyol method [**13**].

Among these techniques, polyol method is particularly attractive due to its short preparation time, low cost, high purity, and the ability to yield excellent crystal qualities. The polyol process has recently been found to be quite useful for direct synthesis of nanocrystalline oxide and chalcogenide materials [**14, 15**]. The background of this method is the precipitation of a solid while heating sufficient precursors in a multivalent and high-boiling alcohol (e.g., diethylene glycol with boiling point of 246°C). Therefore, the alcohol itself acts as a stabilizer, limiting particle growth and prohibiting agglomeration. Due to the high temperatures which can be applied (>150°C) for these high-boiling alcohols, highly crystalline oxides are often formed. Moreover, the synthesis is quite easy to perform. Besides oxides, a variety of materials including sulfides, phosphates, as well as elemental metals have been produced with polyol processes [**16**]. SnO_2 has the rutile-type tetragonal structure belonging to the P42/mnm space group. The lattice parameters are a = b = 4.7382 Å and c = 3.1871Å (JCPDS powder diffraction file), and the band energy-gap is in the ultraviolet range between 3.5 and 3.8 eV as estimated from experimental results and theoretical calculations [**17, 18**].

In this work, after synthesizing of SnO_2 nanoparticles by polyol process, their optical properties have been characterized by UV–vis method. Dominant excitonic peaks are observed in the optical absorption spectra for the first time, which also exhibits a blue shift due to reduction in particle size. Furthermore, the structural characterization is carried out by X-ray diffraction (XRD).

Experimental

Synthesis of SnO_2 nanoparticles

Typically, 125 mL of diethylene glycol (DEG, 99.9%, Aldrich) was first added to a 250 mL round bottomed flask with a reflux condenser. 37.5 millimoles of tin tetra chloride ($SnCl_4$, $5H_2O$), 97%, Aldrich) and appropriate amounts of deionized water were then added into DEG by vigorous stirring. After several hours of heating at 140°C, the resulting suspension was cooled to room temperature. The precipitation was collected by centrifugation. The product was washed with ethanol to remove DEG thoroughly and finally dried in hot-air oven at 80°C.

Characterization

The crystalline quality and the grain size of the samples were evaluated using X-ray diffraction (XRD) measurements. The study was carried out using a (XRD, Bluker D8-Advance) using a Cu Kα1 radiation λ = 1.54056 Å in the θ-2θ geometry. The microstructure and the grain size distribution of the powders were measured by transmission electron microscopy (TEM), using a JEOL 2100F microscope Cs corrected at the probe level, with a point to point resolution of 2.2 Å. For TEM observations, nanopowders were ultrasonically dispersed in ethanol and deposited on amorphous holey carbon membranes.

The surface of the nanoparticles was observed by emission Scanning Eelectron Microscopy (SEM). UV-visible absorption spectra of the samples were studied in the wavelength range 200–1200 nm to determine the band gap using a spectrophotometer. The polycrystalline sample was pressed into pellets of 8 mm diameter and 1.3 mm thickness using 3t/cm^2 uniaxial pressure.

Results and discussion

Structural properties

The X-ray diffraction is used to identify crystalline structure and particle size of the samples. X-ray diffraction patterns of our samples of SnO_2 are shown in **Fig. 1**. The diffraction peaks can be readily indexed to the tetragonal rutile phase of SnO_2 (JCPDS No. 77-0450) [**2**]. However, mostly different ratios of H_2O to precursor salt were investigated. In our studies, we varied the ratio of H_2O : Sn. The best results in terms of small primary crystallite sizes are received when the ratio of H_2O: Sn is 17:1. When H_2O is used in excess, the crystallization rate is very high, which can be seen from the XRD patterns. Therefore, polyol acts as an inhibitor for particle growth. Vice versa, too much water (and certainly OH^- species as well) favors the crystallization and grain growth process.

Moreover, broad peaks were observed in the XRD pattern due to the smaller crystallite size, along with sharp peaks which reveal the good crystalline nature of our samples. Furthermore, the mean grain size (D) and the full width at half maximum (FWHM) of the diffracted line β are related by:

$$D = \frac{0.9\,\lambda}{\beta \cos\theta_\beta} \qquad (1)$$

where, λ is the wavelength of the x-rays used and θ_β is the Bragg angle of the peak in degree. The above equation (1) is known as the Scherrer formula. The results showed that the mean grain size is about 10-30 nm.

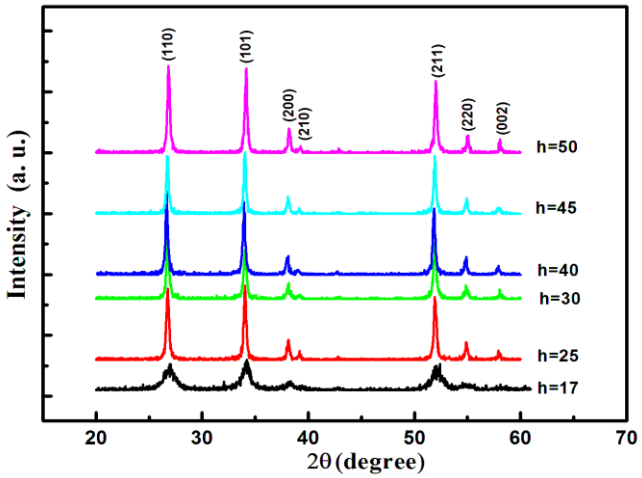

Fig. 1. XRD spectra of SnO_2 nanoparticles with different hydrolysis rate.

Particle size and morphology

The morphology and size of the SnO_2 nanostructures were investigated by SEM. **Fig. 2** shows the detailed morphologies of the SnO_2 low spheres and nanorods with bush-like aggregates with hemispherical ends projecting out.

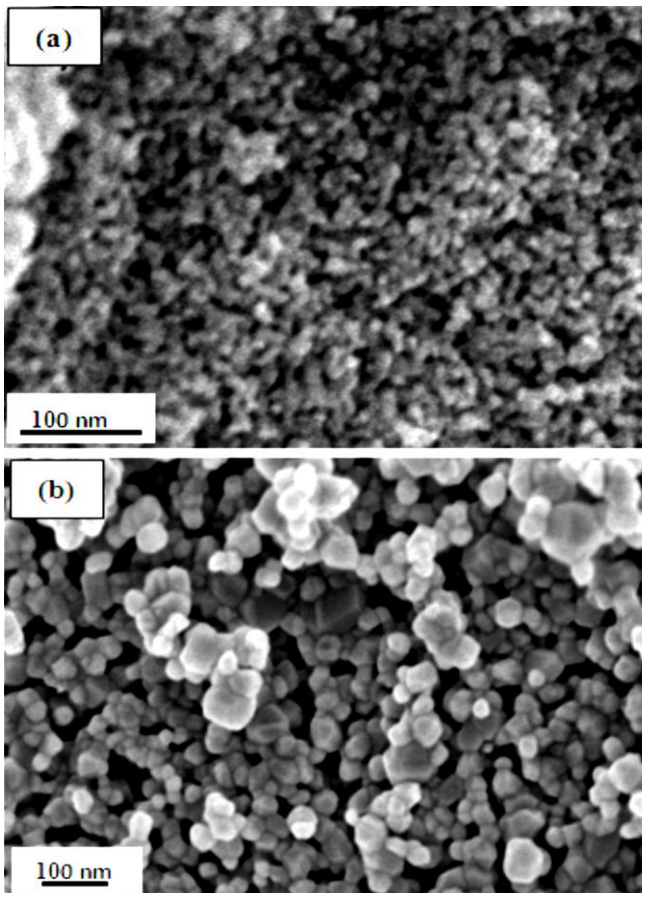

Fig. 2. SEM images of SnO_2 nanoparticles: (a): h= 17 and (b): h=50.

The TEM and SAED photograph of the oxide SnO_2 is given in **Fig. 3**. The photograph shows that the oxide powder is of a composed distribution except for a few aggregated particulates. The average grain size calculated by proportion of the photograph is about 9-12 nm for low hydrolysis rate (**Fig. 3a**). These observations confirmed the small size of the SnO_2 nanoparticles and the obtained values are in good agreement with the size of crystallites calculated from the Scherrer equation. Selected area electron diffraction pattern shows clearly that the powders have crystallized in the rutile phase.

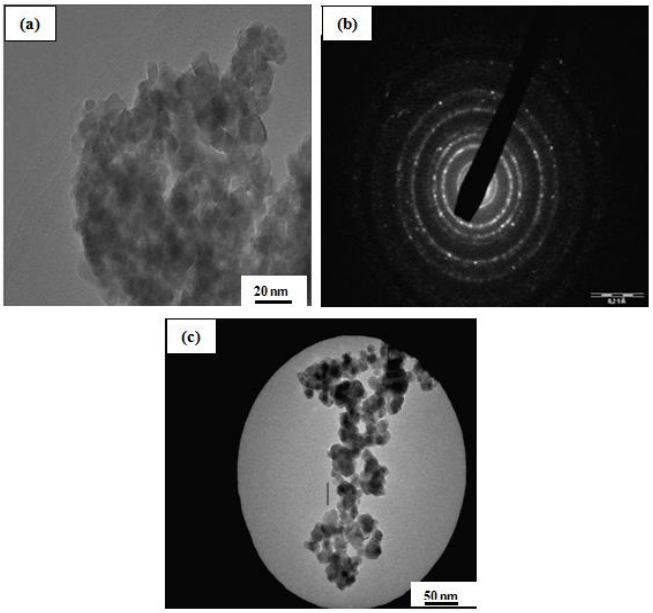

Fig. 3. (a) TEM , (b) SAED images of SnO_2 nanoparticles (h=17) and (c) TEM images of SnO_2 nanoparticles (h=50).

Optical properties

For crystalline SnO_2, optical transition has been shown to be direct **[19]**. The variation in the absorption coefficient as a function of photon energy for allowed direct is given by

$$\alpha(h\nu) = A(h\nu - E_g)^{1/2} \qquad (2)$$

where, α is the absorption coefficient, A is a constant, h is Planck's constant, ν is the frequency, and E_g is the band gap energy. The absorption spectra in the UV and VIS range of SnO_2 nanoparticles with different hydrolysis rate are presented in **Fig. 4**.

All absorption curves exhibit an intense absorption in the 200–420 nm wavelength range and an absorption edge between 300 and 370 nm, owing to the relatively large exciton binding energy. These findings agree well with those obtained by Bouaine *et al.* [**20**].

A plot of $(\alpha h\nu)^2$ versus photon energy was used to obtain the value portion of the curves to zero absorption [21-22]. An attractive result is in relation to the E_g edge from 3.55 to 3.27 eV when hydrolysis rate decrease from h=50 to h=17 in the SnO_2 matrix (**Fig. 5**). This decrease in the energy band gap was already observed in other transition metal oxides and which may be attributed to the decrease in grain size [**23-27**].

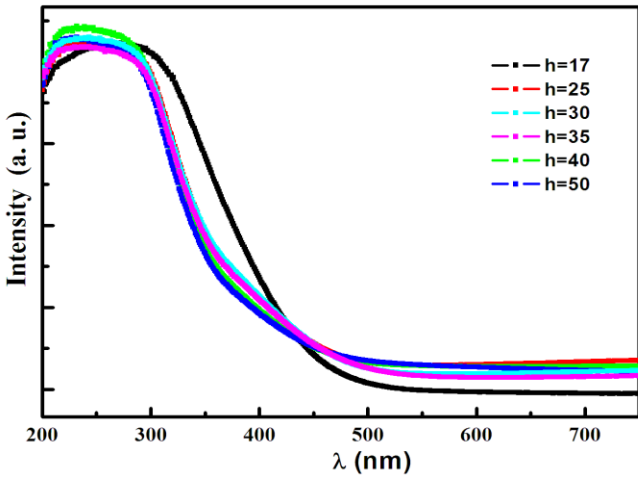

Fig. 4. UV–vis–IR absorption spectrum of SnO_2 nanoparticles with different hydrolysis rate.

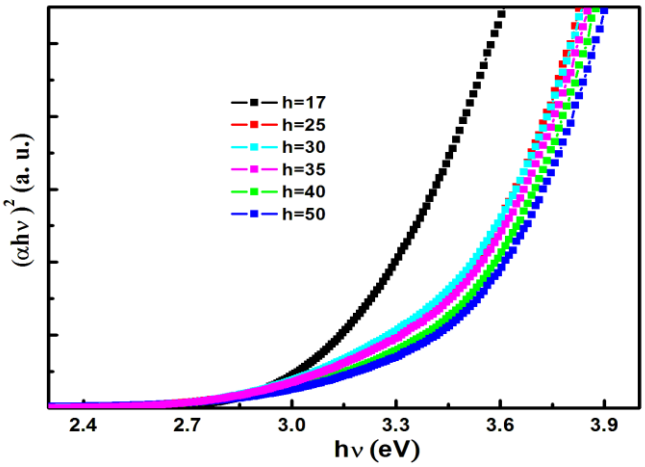

Fig. 5. Plot of $(\alpha h\nu)^2$ versus photon energy (hν) of SnO_2 nanoparticles with different hydrolysis rate.

Fig. 6 shows the typical photoluminescence spectrum of SnO_2 nanoparticles prepared by polyol technique. The appearance of a strong and wide near infrared emission band centered around 447 nm, besides a near band edge emission band, including the bound exciton line which may be attributed to the contribution of oxygen vacancies and defects in the SnO_2 nanoparticles [**28-29**].

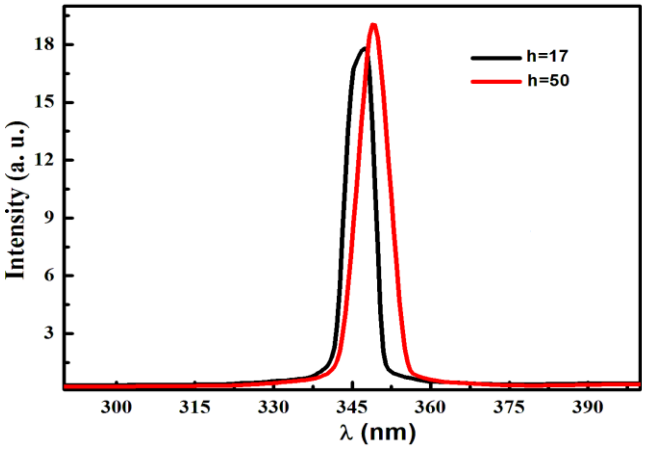

Fig. 6. Typical PL of the final composite SnO_2 at room temperature.

The enhancement in the PL emission can be correlated with the decrease in the grain size observed from the TEM images. In addition, K. Ravichandran *et al.* [**30**] reported that this PL emission in the region of 425–500 nm may be associated with the transition of electrons from oxygen vacancy level to the photo-excited holes in the valence band.

Conclusion

In summary, ultrafine SnO_2 nanocrystalline of 10-30 nm in size were synthesized by using a polyol mediated synthetic method. Their physiochemical properties were then tuned. The XRD analysis revealed that the nanocrystalline are crystallized in tetragonal phase. On the other hand, the X-ray diffraction and TEM show a crystalline phase with a particle size ranging between 10 and 30 nm. The optical band shows an increase with the increase of rate hydrolysis h. PL spectra of the nanopowders show strong luminescence bands located in the visible range green–yellow–red. From the analysis of these results, it can be concluded that this emission attributed to the contribution of oxygen vacancies and defects in the SnO_2 nanoparticles. Consequently, it is important to note that this study opens important perspectives to extend the works to the optical studies of SnO_2 nanoparticles.

Reference

1. Majles, M.; Boroojerdian, P.; Javadi, Z.; Zahedi, S.; Morshedian, M. *Optik*. **2012**,*123*, 2090. **DOI:** 10.1016/j.ijleo.2011.11.005
2. Ahmed, A.; Azam, A.; Shafeeq, M.; Chaman, M.; Tabassum, S. *J. Phys. Chem. Solids*. **2012**, *73*, 943. **DOI:** 10.1016/j.jpcs.2012.02.030
3. Harikrishnan, S.; Kalaiselvam, S. *Thermochim. Acta*. **2012**, *533*, 46. **DOI:** 10.1016/j.tca.2012.01.01
4. Habibzadeh, S.; Beydokhti, A. K.; Khodadadi, A. A.; Mortazavi, Y.; Omanovic, S.; Niassar, M.S. *Chem. Eng. J*. **2010**, *156*, 471. **DOI:** 10.1016/j.cej.2009.11.007
5. Ganguly, S.; Sikdar, S.; Basu, S. *Powder Technol*. **2009**, *196*, 326. **DOI:** 10.1016/j.powtec.2009.08.010
6. Yu, W.; Xie, H.; Chen, L.; Li, Y. *Thermochim. Acta*. **2009**, *491*, 92. **DOI:** 10.1016/j.tca.2009.03.007
7. Mor, G. K.; Carvalho, M. A.; Varghese, M. *J. Mater. Res*. **2004**, *19*, 628. **DOI:** http://dx.doi.org/10.1557/jmr.2004.19.2.628
8. Xiao, L. S.; Shen, H.; Von Hagen, R.; Belkoura, L.; Mathur, S. *Chem. Commun*. **2010**, *46*, 6509. **DOI:** 10.1039/c0cc01156h
9. Bernardi, M. I. B.; Cava, S.; Paiva-Santos, C O.; Leite, E. R.; Paskocimas, C. A.; Longo, Bernardi. *J. Eur. Ceram. Soc*. **2002**, *22*, 2911. **DOI:** PII: S0955-2219(02)00057-2
10. Lan, F.; Wang, X.; Xu, X. *Reac Kinet Mech Cat*. **2012**, *106*, 113. **DOI:** 10.1007/s11144-011-0400-6
11. Zhang, J. R.; Gao, L. *Mater. Chem. Phys*. **2004**, *87*, 10. **DOI:** 10.1016/j.matchemphys.2004.06.004
12. Bargougui, R.; Oueslati, A.; Schmerber, G.; Ulhaq-Bouillet, C.; Colis, S.; Hlel, F.; Ammar, S.; Dinia, A. *J Mater Sci: Mater. Electron*. **2014**, *25*, 2066. **DOI:** 10.1007/s10854-014-1841-2
13. Jung, D.; Dong,W. *P. Appl. Surf. Sci*. **2009**, *255*, 5409. **DOI:** 10.1016/j.apsusc.2008.08.054
14. Toneguzzo, P.; Viau, G.; Acher, O.; Fievet-Vincent, F.; and Fievet, F.; *AdV. Mater*. **1998**, *10*, 1032. **DOI:** 10.1002/(SICI)15214095(199809)
15. Grisaru, H.; Palchik, O.; Gedanken, A.; Palchik, V.; Slifkin, M.; Weiss, *A. Inorg. Chem*. **2003**, *42*, 7148. **DOI:** 10.1021/ic0342853
16. Feldmann, C.; Metzmacher, C. *J. Mater. Chem*. **2001**, *11*, 2603. **DOI:** 10.1039/B100818H
17. Kirszensztej, P.; Tolinska, A.; Przekop, R. *J. Therm Anal Calorim*. **2009**, *95*, 93. **DOI:** 10.1007/s10973-008-9085-0
18. Ogale, S.B.; Choudhary, R.J.; Buban, J.P.; Lofland, S.*E. Phys. Rev. Lett*. **2003**, *91*, 077205. **DOI:** 10.1103/PhysRevLett.91.077205
19. Robertson, J. *J. Phys .C*. **1979**, *12*, 4767. **DOI:** 10.1088/0022-3719/12/22/018
20. Bouaine, A.; Brihi, N.; Schmerber, G.; Ulhaq-Bouillet, C.; Colis, S.; Dinia, A. *J. Phys. Chem. C* . **2007**, *111*,2924. **DOI:** 10.1021/jp066897p
21. Tauc, J.; Grigorovici, R.; Vancu, A. *Phys. Stat. Sol*. **1966**, *15*, 627. **DOI:** 10.1002/pssb.19660150224
22. Luo, S.; Fan, J.; Liu, W.; Zhang, M.; K Chu, P. *Nanotechnology*. **2006**, *17*, 1695. **DOI:** 10.1088/0957-4484/17/6/025
23. Bouloudenine, M.; Viart, N.; Colis, S.; Dinia, A. *Chem. Phys. Lett*. **2004**, *73*, 397. **DOI:** 10.1016/j.cplett.2004.08.064
24. Colis, S.; Bieber, H.; Bégin-Colin, S.; Schmerber, G.; Leuvrey, C.; Dinia, *A. Chem. Phys. Lett*. **2006**, *422*, 529. **DOI:** 10.1016/j.cplett.2006.02.109
25. Gu, F.; Wang, S.F.; Lv, M.K.; Qi, Y.X.; Zhou, G.J.; Xu, D.;Yuan, D.*R. Inorg. Chem.Commun*. **2003**, *6*, 882. **DOI:** 10.1016/S1387-7003(03)00135-7
26. Zhao, Q.; Li, Z.; Wu, C.; Bai, X.; Xie, Y. Journal of Nanoparticle Research. 2006, 8 1065. **DOI:** 10.1007/s11051-006-9110-9
27. Bouazizi, N. ; Bargougui, R.; Oueslati, A. ; Benslama, R. ; *Adv. Mater. Lett*. **2015**, *6(2)*, 158-164. **DOI:** 10.5185/amlett.201 5.5656
28. Marcano, D. C.; Kosynkin, D.V.; Berlin, J. M.; Sinitskii, A.; Sun, Z.; Slesarev, A.; Alemany, L. B.; Lu, W.; Tour, J. M.; *ACS. Nano*. **2010**, *4*, 4806. **DOI:** 10.1021/nn1006368
29. Zou, G.; Li, H.; Zhang, D.; Xiong, K.; Dong, C.; Qian, Y. *J. Phys. Chem.B.***2006**, 1632, 1637. **DOI:** 10.1021/am201663d
30. Ravichandran, K.; Thirumurugan, K.; Jabena Begum, N.; Snega, *S. Superlattices and Microstructures013*, *60*, 327. **DOI:** 10.1016/j.spmi.2013.05.006

